This draft is published as "Effects of surface strain on oxygen adsorption on Zr (0001) surface", X. Wang, M. Khafizov, I. Szlufarska, Journal of Nuclear Materials, 2014

Effect of surface strain on oxygen adsorption on Zr (0001) surface

X. Wang [a], M. Khafizov [b], I. Szlufarska [a, c, *]

[a] Department of Engineering Physics, University of Wisconsin-Madison, 1500 Engineering Drive, Madison, WI 53706, USA

[b] Idaho National Laboratory, Idaho Falls, ID 83415, USA

[c] Department of Materials Science and Engineering, University of Wisconsin-Madison, 1509 University Avenue, Madison, WI 53706, USA

* Corresponding author. Tel.: +1 608 265 5878

Email addresses: xwang348@wisc.edu (X. Wang), marat.khafizov@inl.gov (M. Khafizov), szlufarska@wisc.edu (I. Szlufarska)

Abstract

The effect of surface strain on oxygen adsorption on Zr (0001) surface is investigated by density functional theory (DFT) calculations. It is demonstrated that both surface strain and interactions between oxygen adsorbates influence the adsorption process. Oxygen binding to zirconium becomes stronger as the strain changes from compressive to tensile. When oxygen coverage is low and the oxygen interactions are negligible, surface face-centered cubic sites are the most stable for O binding. At high coverage and under compression, octahedral sites between second and third Zr layers become most favorable because the interactions between adsorbates are weakened by positive charge screening. Calculations with both single-layer adsorption model and multiple-layer adsorption model demonstrate that compressive strain at the Zr/oxide interface will provide a thermodynamic driving force for oxygen to incorporate from the surface into the bulk of Zr, while binding oxygen to the Zr surface will be easier when tensile strain is applied.

1. Introduction

Zirconium alloys have been widely used as cladding materials for water-cooled reactors because of the low thermal neutron capture cross section and a reasonable corrosion resistance of these materials. However, corrosion is still one of the major reasons for the degradation of Zr alloys during service [1]. Consequently, understanding the oxidation mechanism of Zr is of great theoretical and technological interest. Investigating the adsorption of oxygen on Zr surface is the first step toward understanding of initial oxidation kinetics and it is therefore not surprising that a number of studies have been focused on this topic. For example Wang and co-authors [2-4] carried out a low-energy electron diffraction (LEED) study on Zr (0001) surface and proposed a so-called double-layer adsorption model. In this model, when the oxygen coverage is 0.5 monolayer (ML) or 1 ML, half of the oxygen atoms will occupy the octahedral sites between the first and the second Zr layer while the other half will reside on the octahedral sites between the second and third layer. However, when oxygen coverage increases to 2 ML, it becomes more favorable for half of the O atoms to occupy the surface face-centered cubic sites and the rest to reside on the tetrahedral sites between the first and the second metal layer just above the second Zr layer. On the simulation side, density functional theory (DFT) calculation of Yamamoto *et al.* [5] found that energetically the most favorable sites on Zr(0001) surface are the octahedral sites between the second and the third Zr layers. These calculations were performed with local density approximation (LDA). Interestingly, DFT calculation by two other groups [6, 7] based on the generalized gradient approximation (GGA) suggested that it is the surface face-centered cubic sites that are energetically more stable. The authors of Ref. [7] also proposed a multiple-layer adsorption model. According to this model the most stable configuration is the one in which O atoms occupy surface face-centered cubic sites and alternate octahedral sites between Zr layers at the same time. The arrangement of O adsorbates in this case is driven by interactions between these atoms, which are repulsive and therefore the atoms prefer to stay as far as possible from each other.

The above studies have provided many key insights into the adsorption process of oxygen on Zr surface, but one important aspect that has not be addressed yet is the effect of stress and strain on the oxygen adsorption. It is known that as the oxide scale grows laterally, a dense zirconia layer is formed on the metal surface [1]. This oxide film, which consists of metastable tetragonal phase and stable monoclinic phase of zirconia [8], acts as a protective layer for zirconium against further corrosion [9, 10].

Due to the lattice mismatch, large planar stress is built up at the metal/oxide interface. The stress is compressive for oxide and tensile for zirconium [9, 11, 12]. This stress (or equivalently strain) is believed to stabilize the metastable tetragonal oxide (t-ZrO_2). This modifies the chemical reactivity of the interface and thus has a significant impact on the oxidation process [10, 11]. There have been many studies focusing on the strain effect on diffusivity of oxygen ions in Zr-O systems. For example, Barriocanal *et al.* found that the ionic conductivity of yttria stabilized zirconia (YSZ) ultrathin films is enhanced by eight orders of magnitude when the YSZ films are coherently "strained" between SrTiO3 layers at room temperature [13]. Kushima *et al.* performed DFT and Monte Carlo simulations of YSZ with up to 8% tensile strain and found the maximum enhancement in diffusivity was 6.8×10^3 at strain of 4% and 400 K [14]. DFT calculations of Hirschfeld *et al.* have shown that the migration barrier for oxygen ions in cubic ZrO_2 initially increases with compressive strain (up to 9%) and then decreases at high compressive strains (up to 15%) [15]. An increase in migration barriers for compressive strains up to 5% in tetragonal ZrO_2 has also been found in a study based on empirical potentials and temperature accelerated dynamics [16]. The same author found that for the tensile conditions, migration barrier decreases with up to 1%, but then increases at larger strain. However, the effects of surface strain on oxygen adsorption on zirconium surface have not yet been considered. Here, we report DFT calculations of this effect for Zr (0001) surface and we demonstrate how strain effect couples to oxygen coverage. We consider compressive and tensile strains up to 6.6%. Tensile strain is expected due to the lattice mismatch between the metal and the oxide, whereas residual compressive strain can be present due to defects and due to stresses exerted on Zr in engineering applications. It is important to point out that under larger compressive strains the hcp Zr will transform into other phases (see section 2) and consideration of the hcp phase in 5.0% ~ 6.6% strain is not physical. However, as we show later in this paper, there is a merit to extending calculations to these large strains because they help elucidate the physical origins of the trends and phenomena observed at smaller strain.

2. Computational methods

DFT calculations were performed with the projected augmented wave (PAW) [17] method and using the Vienna *Ab Initio* Simulation Package (VASP) [18, 19]. GGA was adopted to describe electron exchange and correlation. It is known that LDA shows over-binding for chemical reactions at surfaces, and this effect is largely corrected by GGA [20]. The cut-off energy was 400 eV for plane wave set. During the calculation, atoms were fully relaxed until all forces acting on ions were lower than 0.01 eV/Å. By fully relaxing the bulk Zr supercell, we found the lattice constants for pure hcp Zr to be a=3.233 Å and c=5.181 Å, which agreed well with previous experiments [21] and DFT calculations [22]. The Zr (0001) surface was modeled by a periodic slab that consisted of nine Zr layers separated by a vacuum region,

which had a thickness equivalent to that of seven bulk Zr layers (18.134 Å). All the atoms were allowed to move except the three Zr layers at the bottom. To obtain different oxygen coverages, (2×2), (3×3) and (4×4) surface cells were adopted in the simulation. Here the notation (n×n) means the surface lattice vectors are n-multiples of the basis vectors of the bulk unit cell along the truncated surface. For (2×2), (3×3) and (4×4) surface cells, wave functions were expanded at Γ point in Brillouin zone (BZ) by 9×9×1, 7×7×1 and 5×5×1 Monkhorst-Pack k point-meshes, respectively. We also increased the number of Zr layers and number of k-point to make sure that our calculations are converged with current settings.

The geometries of different binding sites for oxygen are shown in Fig. 1. We adopt the same notations as in Ref [7]. SFCC means surface face-centered cubic sites. SHCP refers to surface hexagonal close-packed sites. Octa*ij* represents the octahedral sites between i^{th} and j^{th} Zr layer. To avoid artificial dipole moments due to oxygen adsorption on one side of Zr slab in the calculations, dipole corrections were introduced using the IDIPOL tag in VASP [23].

The binding energy E_b of an oxygen atom is defined as

$$E_b(\theta) = \frac{E_{total}^{slab}(\theta) - E_{total}^{Zr\ slab}}{N_{oxygen}} - \frac{1}{2}E_{O_2} \quad , \tag{1}$$

where θ is the oxygen coverage, defined as the ratio of the number of adsorbed oxygen atoms to the number of Zr atoms in the surface layer. $E_{total}^{slab}(\theta)$ and $E_{total}^{Zr\ slab}$ are the total energies per unit cell of the Zr slab with and without adsorbed oxygen, respectively. N_{oxygen} is the total number of adsorbed oxygen atoms and E_{O_2} is the reference energy of oxygen molecule calculated from DFT. To calculate E_{O_2}, an oxygen dimer was fully relaxed in a cubic box of vacuum with 10 Å side length. The final E_{O_2} energy is -8.76 eV.

In the simulation, biaxial strain is defined as

$$\varepsilon = \ln(\frac{x'}{x}) = \ln(\frac{y'}{y}) \quad , \tag{2}$$

where x and y represent the dimensions of the unit cell without strain, and x' and y' are the corresponding dimensions under strained conditions. Both, compressive (defined as negative) and tensile (defined as positive) biaxial strains were applied to the supercell. It should be noted that hcp zirconium metal would transform into other phases under high temperature/pressure conditions. For pressures larger than 5.6 GPa, the hcp ($P6_3/mmc$) phase is no longer stable and it adopts ω (P6/mmm) phase [24]. Based on the elastic constants of the Zr hcp crystal [22], this stress corresponds to about 5.0% biaxial strain, which is smaller than the maximum strain of 6.6% applied in our simulation. Consequently, only calculations with strains up to 5.0% should be viewed as providing results that can be observed experimentally. All important

relative stability changes of different adsorption structures in our calculation occurred within this strain range. Larger strains in this study are considered to provide insights into the physical origins of the observed phenomena.

The energy calculated from DFT methods corresponds to zero temperature, while the normal operation temperature for zirconium cladding tubes in nuclear reactors is about 300-360 ℃ [1]. To include the temperature effects, we add a vibrational free energy (G_{vib}) term to the zero-temperature *ab initio* energy in Eq. (1). We assume the vibrational terms of the Zr slab do not change significantly upon insertion of oxygen atoms, and therefore these terms are mostly cancelled when calculating the binding energy. As a result, the main contribution to vibrational free energy comes from oxygen, which changes from the O_2 gas phase to isolated O ions in the Zr solid. Following references [25, 26], the binding energy at temperature *T* is calculated as

$$E_b(\theta,T) = \frac{E_{total}^{slab}(\theta) - E_{total}^{Zr\ slab}}{N_{oxygen}} - \frac{1}{2}(E_{O_2} + \Delta G_{vib}(O_2,T)) \quad , \tag{3}$$

Here, we choose the reference temperature *T* = 633.15 K (360 ℃) and obtain $\Delta G_{vib}(O_2,T) = -0.92\,eV$. In this notation more negative binding energy indicates a stronger binding.

3. Results and discussion

3.1 The relative stability of different adsorption sites under strain

Previous DFT calculations demonstrated that tetrahedral sites between Zr layers are less energetically favorable than octahedral sites [5-7]. Therefore, we mainly focus on the strain effects on the binding energy of octahedral, SFCC and SHCP sites. The oxygen binding energy of different adsorption sites under different strain conditions are summarized in Table 1 and Fig. 2. At zero strain, the relative stability of different adsorption sites is consistent with previous calculations with GGA [6, 7]. According to Fig. 2, E_b becomes more negative, which means a stronger binding, as the strain changes from compressive to tensile. This trend can be justified based on geometric considerations, as the tensile strain increases the free volume between Zr atoms increases and provides more space for an interstitial oxygen atom. The opposite is true under compressive strain and therefore it is not surprising that oxygen is less stable under such conditions. However, in terms of the relative stability of specific adsorption sites, there is something more interesting happening when the Zr slab is compressed. The increase of binding energy (to less negative values and therefore to lower stability) is more pronounced for surface sites (SFCC and SHCP) than for bulk sites (Octa23 and Octa34), eventually leading to surface sites becoming less stable at about ε=-4.2%. This trend is surprising because the spacing between Zr atoms will decrease as compressive strain applied. Since on the surface, O atoms have more freedom to shift toward or away from the surface,

one would expect that the effect of compressive strain on surface sites would be smaller than in the bulk where O atoms are confined in all three spatial directions. It is the opposite trend to what we observe in our simulations.

We hypothesize that the possible origin of the larger stability of bulk sites under compressive strain is interaction between oxygen atoms, which may be different in the bulk and on the surface of the Zr metal. To test this hypothesis, we calculated E_b for different coverage θ for SFCC and Octa23 sites, which we choose as the representatives of adsorption sites on the surface and in the bulk, respectively. The results are summarized in Table 2 and Fig. 3. As the data shows, oxygen binding energy decreases as coverage θ changes from high to low, which is consistent with the fact that the interaction between the oxygen adsorbates is repulsive and demonstrates that this interaction plays an important role in adsorption. By comparing binding energies at the same strain, it is clear that the effect of surface coverage on E_b weakens as the coverage becomes small. This effect eventually becomes negligible, as we find binding energies for θ=1/9 ML and θ=1/16 ML to be within 0.05 eV of each other, for both SFCC and Octa23 sites. We can therefore assume that oxygen interaction can be neglected at θ=1/16 ML and only the pure geometric effect of strain on oxygen absorption is left. As shown in Fig. 3 by the dashed lines for SFCC and Octa23 sites, under this condition, SFCC (surface) sites would always be more stable than bulk sites, even when under a large compressive strain. In addition, if we calculate $\Delta E = E_b(\varepsilon=-6.6\%) - E_b(\varepsilon=0.0\%)$ as a measure for the sensitivity to compressive strain at θ=1/16 ML, we obtain that ΔE=0.39 eV for Octa23, which is bigger than ΔE=0.21 eV for SFCC. This result implies that Octa23 (bulk) sites are more sensitive to compressive strain than SFCC (surface) site, which is consistent with the intuitive picture that surface sites provide more free volume for O adsorbates than bulk under the same compressive strain and therefore O should be more stable at the surface.

Based on the above calculations, the change of E_b under general strain conditions can be attributed to two dominant factors**:** surface strain and adsorbate interactions. When coverage of oxygen is high and large compressive strain is applied, oxygen-oxygen interaction dominates and changes the order of stability of different adsorption sites. On the other hand, when θ is low and oxygen-oxygen interaction could be neglected, E_b will be only affected by the geometry and the availability of free volume for O within the Zr structure.

3.2 Bulk sites vs. surface sites

Since surface sites and bulk sites exhibit different responses to a biaxial strain, it is instructive to discuss in more detail trends observed for the two kinds of adsorption sites. For Octa23 (bulk sites), at low coverage (θ=1/9 ML), E_b increases notably when under compressive strain, but remains relatively

constant under tensile conditions. The behavior under tensile conditions can be understood again by considering free volume available for O interstitials. As tensile strain increases, more interstitial space will be available for oxygen. However, at a certain strain interstitial space between Zr atoms will be sufficiently large for oxygen interstitials so that increasing this space further by strain will no longer have a significant effect on stabilizing the oxygen adsorbates. At an intermediate coverage (θ=1/4 ML), the E_b curve overlaps with the curve of θ=1/9 ML as the strain changes from -6.6% to 3.3%. This trend means that oxygen interactions do not play an important role until the absolute value of the compressive strain ε is larger than 3.3%. At high coverage (θ=1 ML), E_b is always about 0.4 eV larger than E_b at low coverage at the same strain. It implies that adsorbate interactions appear and become the dominant contributor at tensile conditions.

For SFCC (surface sites) at low coverage (θ=1/9 ML), E_b decreases almost linearly from strain of -6.6% to +6.6%. As the oxygen coverage increases to θ=1/4 ML, unlike the bulk sites, oxygen interaction begins to have finite values at the lowest compressive strain considered in our study, which is shown by the deviation of E_b curve of θ=1/4 ML from the one of θ=1/9 ML in Fig. 3. This onset of the contributions from the O – O interactions occurs earlier than for Octa23, where compressive strain of ε=-3.3% was required to observe a similar effect. At high coverage (θ=1 ML), oxygen interactions appear even under tensile conditions, which is similar to the case of Octa23.

As discussed in preceding paragraphs, when coverage is lower than 1/9 ML, the relation between the binding energy and the strain is entirely dominated by geometric effects (i.e., the availability of free volume). Consequently, we can estimate the contribution from interaction energy $E_{O\text{-}O}$ between oxygen atoms to the binding energy, by subtracting E_b at θ=1/16 ML from E_b at a higher oxygen coverage. We also measured the distance between oxygen atoms, $d_{O\text{-}O}$, under different coverage conditions. $d_{O\text{-}O}$ are the same (within 0.001 Å) for SFCC and Octa23 when strain and coverage are equal. Therefore, we can plot O-O interaction energy of SFCC and Octa23 sites as a function of O-O distance (see Fig. 4). As expected for repulsive interactions, the oxygen interaction energy increases as oxygen distance decreases. In addition, $E_{O\text{-}O}$ for SFCC increases much faster than that of Octa23. Again, this analysis shows that oxygen interactions have a larger effect on the adsorption process on surface sites than bulk sites, especially when coverage is high. To demonstrate that the aforementioned phenomena and analysis are general and applicable to other binding sites, we also calculate E_b of SHCP (surface) and Octa34 (bulk) for coverage ranging from θ=1/4 ML to 1 ML and with strain within the ± 6.6% range. As shown in Fig. 5, the results have the same trends as those observed for SFCC vs. Octa23 (Fig. 3).

It is interesting to ask why oxygen interaction is larger for the surface than for the bulk. The reason might be the different electronic properties of oxygen in these two configurations. For surface adsorption sites (SFCC and SHCP), each oxygen atom has three nearest Zr neighbors and the negative charge around O is partially screened. However, for oxygen atoms on bulks sites, such as Octa23, each oxygen atom is located in the center of the octahedron formed by six nearest zirconium neighbors. As a result, one can expect that in the bulk oxygen charge is more effectively screened by the surrounding metal and the interactions between oxygen adsorbates are therefore weaker than on the surface. A similar difference in screening effects between surface and bulk sites was also reported in (Ga,Mn)As system [27].

It is instructive to consider the impact of surface strain on the early stages of Zr oxidation. The early oxidation process can be divided into three successive steps. First, oxygen molecules dissociate from the gas phase and bind as monoatomic oxygen to the Zr surface. Subsequently, as the coverage of oxygen increases, some oxygen ions diffuse as interstitials deeper into the Zr layers, and finally nucleation of new oxide phases takes places in the near surface region of the Zr metal. In the first stage, since binding energy becomes more negative (indicating stronger adsorption) as the strain changes from compressive to tensile, adsorption of oxygen to the Zr surface would be accelerated under tension and decelerated under compression. The diffusion stage depends on both thermodynamic (i.e., the difference in binding energies) and kinetic (i.e., migration energies) factors. For conditions of large compressive strain and high oxygen coverage, due to the interaction between oxygen adsorbates, surface sites become less stable than bulk sites. This phenomenon provides a strong thermodynamic driving force for oxygen ions to migrate deeper into zirconium. For tensile conditions, surface sites become more stable than bulk sites, so that the thermodynamic driving force for oxygen incorporation is reduced. However, since strain is also likely to affect migration barriers of oxygen in Zr, kinetic effects need to be considered before definitive conclusions can be reached regarding strain effects on oxygen incorporation into Zr. The oxide nucleation stage of Zr oxidation depends on the free energies of the different oxide phases, on the energies of oxide/Zr interface and on the amount of strain introduced into the Zr lattice upon nucleation. The effects of biaxial strain in Zr on these properties remain unknown.

3.3 Strain effects on oxygen adsorption sites in multiple layers

As discussed in Section 1, both single-layer adsorption model (SLAM) and multiple-layer adsorption model (MLAM) have been proposed in literature. In the latter model, oxygen atoms can occupy adsorption sites in different layers at the same time, instead of residing in one monolayer. Given the important role of oxygen interactions on adsorption, it is not surprising that oxygen atoms prefer to stay away far from each other and be distributed among different Zr layers. One can ask if this trend will change when Zr is under strain, as considered in our study. Here, we address this question by

investigating different structures of MLAM when oxygen coverage is equivalent to 2.0 ML and under compression. We use (2×2) surface cell so 2.0 ML means eight adsorbed oxygen atoms. The results are shown in Fig. 6. Eight different adsorption structures (SFCC+Octa23, Octa23+Octa45 etc.) were considered. In each structure, oxygen atoms are distributed among the different layers as evenly as possible. For example, SFCC+Octa23+Octa45+Octa67 means that oxygen atoms occupy these four kinds of adsorption sites and there are two oxygen atoms in each layer. Different arrangements of oxygen atoms among possible adsorption sites were tested and the oxygen binding energy of the most stable configuration in each adsorption structure is reported here.

We compare predictions of our simulations to existing experiments. Specifically, the authors of Ref. [4] reported the results of LEED experiments applied to investigate the oxygen adsorption structure for θ=2.0 ML. In these experiments, the diffraction intensity – incident electron energy curve of Zr (0001) surface with 2 ML oxygen was recorded and compared to curves calculated theoretically for thirty plausible adsorption structures. The agreement was quantified using the so-called R_p factor. The lowest value of R_p factor (which means the best match for the experiment data) was found for the structure of SFCC+Tetra12_a2 (tetragonal sites between the first and the second metal layers just above the second Zr layer). This conclusion is seemingly contradictory to our finding that the lowest-energy adsorption site is SFCC+Octa23+Octa45+Octa67. To understand the apparent discrepancy, we calculated the oxygen binding energy of all three structures from Ref. [4] that had R_p factor lower than 0.400, including the SFCC_Tetra12_a2 structure (see open symbols in Fig. 6). At zero strain, the SFCC+Tetra12_a2 has the lowest binding energy among the three structures, which shows that our calculation is consistent with the LEED results. However, the energy of this structure is higher than the energies of the other O arrangements considered in our study and also shown in Fig. 6. This is because the authors of Ref. [4] focused on possible adsorption structures that put O atoms into adjacent adsorption layers (such as SFCC+Tetra12_a2, SFCC+Octa12, SFCC+Octa12+Octa23). If, on the other hand, one entire layer of adsorption sites is left empty, as for example in SFCC+Octa23, the distance between O atoms along the direction perpendicular to the surface is increased. Such arrangement reduces the repulsion between oxygen adsorbates and leads to a lower E_b, as shown in Fig. 6. Of course, one should keep in mind that the binding energy only indicates the relative thermodynamic stability between different adsorption structures. Kinetically, the migration barrier for oxygen diffusing across Zr layers might be too high, so that oxygen adsorbates may still prefer to stay in the first two adsorption layers (such as SFCC+Tetra12_a2) when the coverage is θ=2.0 ML.

Similarly as for the SLAM, in MLAM oxygen binding energy is more negative (oxygen becomes more stable) at zero strain than that at compressive strain. We also observe some additional changes in the

relative stability between different adsorption sites when a large compressive strain is applied. When ε=0%, surface and near-surface sites (SFCC+Octa23) are more stable than the sites that are away from the surface and deeper in the bulk (Octa23+Octa45). This order changes as compressive strain is applied, which again can be explained by different electron screening for surface and bulk sites (see section 3.2). All of these trends are qualitatively the same as those found by us for the SLAM model discussed earlier. In general, our results show that at any strain condition, the further separated the oxygen ions are from each other within the Zr metal, the more stable the structure will be. Consequently, at the early stage of oxidation, as more and more oxygen are adsorbed on the Zr surface, some of them will be incorporated into deeper Zr layers.

4. Conclusions

Ab initio calculation was performed to investigate the oxygen adsorption on strained Zr (0001) surface. Both geometric effects and adsorbate interactions are shown to have important contributions to the changes of oxygen binding energy with strain. At very low coverage of oxygen, bulk sites are more sensitive to surface strain than surface sites. However, when oxygen coverage is high and oxygen interactions become dominant, surface sites become less favorable as binding sites than bulk and therefore compressive strain provides a thermodynamic driving force for oxygen to diffuse into deeper Zr layers. Multi-layer and single-layer adsorption models show similar qualitative trends with strain and these trends can be explained by the same physics.

Acknowledgements

This work was supported through INL Laboratory Directed Research & Development (LDRD) Program under DOE Idaho Operations Office Contract DE-AC07-05ID14517. The authors also gratefully acknowledge use of computational facilities supported by the University of Wisconsin Materials Research Science and Engineering Center (DMR-1121288). We would like to thank Dr. Chao Jiang from Computational Materials Group, UW-Madison for helpful discussions.

Reference

[1] B. Cox, J. Nucl. Mater. 336 (2005) 331-368.
[2] Y.M. Wang, Y.S. Li, K.A.R. Mitchell, Surf. Sci. 343 (1995) L1167-L1173.
[3] Y.M. Wang, Y.S. Li, K.A.R. Mitchell, Surf. Sci. 342 (1995) 272-280.
[4] Y.M. Wang, Y.S. Li, K.A.R. Mitchell, Surf. Sci. 380 (1997) 540-547.
[5] M. Yamamoto, C.T. Chan, K.M. Ho, S. Naito, Phys. Rev. B 54 (1996) 14111-14120.
[6] G. Jomard, A. Pasturel, Appl. Surf. Sci. 177 (2001) 230-237.

[7] F.H. Wang, S.Y. Liu, J.X. Shang, Y.S. Zhou, Z.Y. Li, J.L. Yang, Surf. Sci. 602 (2008) 2212-2216.
[8] A. Yilmazbayhan, E. Breval, A.T. Motta, R.J. Comstock, J. Nucl. Mater. 349 (2006) 265-281.
[9] M.G. Glavicic, J.A. Szpunar, Y.P. Lin, J. Nucl. Mater. 245 (1997) 147-151.
[10] A.P. Zhilyaev, J.A. Szpunar, J. Nucl. Mater. 264 (1999) 327-332.
[11] H.L. Li, M.G. Glavicic, J.A. Szpunar, Mater. Sci. Eng. A-Struct. Mater. Prop. Microstruct. Process. 366 (2004) 164-174.
[12] H. El Kadiri, Z.N. Utegulov, M. Khafizov, M. Asle Zaeem, M. Mamivand, A.L. Oppedal, K. Enakoutsa, M. Cherkaoui, R.H. Craham, A. Arockiasamy, Acta Mater. 61 (2013) 3923-3935.
[13] J. Garcia-Barriocanal, A. Rivera-Calzada, M. Varela, Z. Sefrioui, E. Iborra, C. Leon, S.J. Pennycook, J. Santamaria, Science 321 (2008) 676-680.
[14] A. Kushima, B. Yildiz, J. Mater. Chem. 20 (2010) 4809-4819.
[15] J.A. Hirschfeld, H. Lustfeld, Phys. Rev. B 84 (2011) 224308.
[16] X.M. Bai, Y.F. Zhang, M.R. Tonks, Phys. Chem. Chem. Phys. (2013) accepted.
[17] P.E. Blochl, Phys. Rev. B 50 (1994) 17953-17979.
[18] G. Kresse, J. Furthmuller, Phys. Rev. B 54 (1996) 11169-11186.
[19] G. Kresse, J. Furthmuller, Comp. Mater. Sci 6 (1996) 15-50.
[20] A. Gross, Theoretical surface science : a microscopic perspective, Springer, Berlin ; New York, (2003) pp. 40-43.
[21] A.I. Kolesnikov, A.M. Balagurov, I.O. Bashkin, A.V. Belushkin, E.G. Ponyatovsky, M. Prager, J Phys-Condens Mat, 6 (1994) 8977-8988.
[22] B.T. Wang, P. Zhang, H.Y. Liu, W.D. Li, P. Zhang, J. Appl. Phys. 109 (2011) 063514.
[23] L. Bengtsson, Phys. Rev. B 59 (1999) 12301-12304.
[24] D.A. Young, Phase diagrams of the elements, University of California Press, Berkeley, 1991, pp. 170-172.
[25] Y.L. Lee, J. Kleis, J. Rossmeisl, D. Morgan, Phys. Rev. B 80 (2009) 224101.
[26] Y.L. Lee, D. Morgan, Phys. Chem. Chem. Phys. 14 (2012) 290-302.
[27] J. Fujii, M. Sperl, S. Ueda, K. Kobayashi, Y. Yamashita, M. Kobata, P. Torelli, F. Borgatti, M. Utz, C.S. Fadley, A.X. Gray, G. Monaco, C.H. Back, G. van der Laan, G. Panaccione, Phys. Rev. Lett. 107 (2011) 187203.

Table1.
Oxygen binding energy of different binding sites as a function of strain under θ =1 ML oxygen coverage

Strain	SFCC	SHCP	Octa12	Octa23	Octa34
-6.6%	-4.68	-4.61	-4.61	-4.85	-4.84
-3.3%	-5.11	-4.95	-4.72	-5.06	-5.03
0.0%	-5.41	-5.21	-4.73	-5.19	-5.11
3.3%	-5.55	-5.35	-4.75	-5.21	-5.15
6.6%	-5.58	-5.40	-4.75	-5.14	-5.14

Table 2
Binding energy E_b (eV) of oxygen on SFCC and Octa23 sites with different oxygen coverage θ (ML) and strain conditions

	Surface (SFCC)				Bulk (Octa23)			
strain	θ=1	θ=1/4	θ=1/9	θ=1/16	θ=1	θ=1/4	θ=1/9	θ=1/16
-6.6%	-4.68	-5.40	-5.64	-5.61	-4.85	-5.15	-5.27	-5.26
-3.3%	-5.11	-5.63	-5.71	-5.78	-5.06	-5.49	-5.50	-5.50
0.0%	-5.41	-5.85	-5.84	-5.88	-5.19	-5.65	-5.66	-5.64
3.3%	-5.55	-5.99	-5.93	-5.96	-5.21	-5.66	-5.69	-5.67
6.6%	-5.58	-6.09	-6.05	-6.08	-5.14	-5.64	-5.65	-5.71

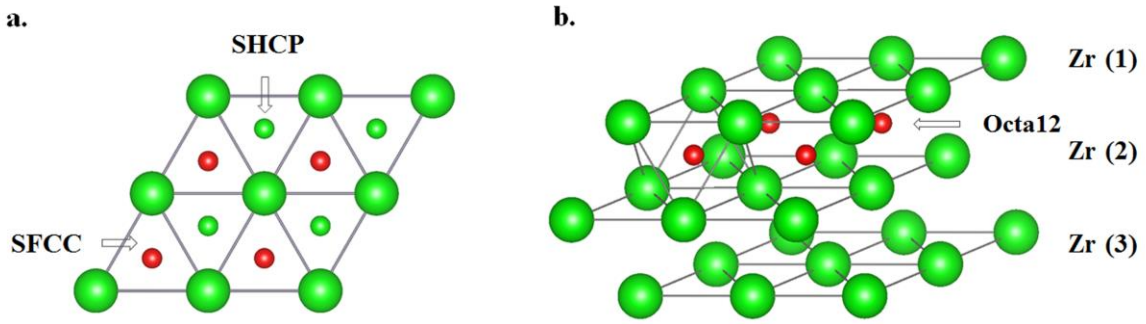

Fig. 1. (color online) Illustration of different binding sites. (a) Top view of (3×3) supercell. Large green circles represent Zr atoms within the 1st (surface) layer; small red circles represent SFCC oxygen; small green circles represent SHCP oxygen atoms. Zr atoms in the 2nd layer are directly underneath SHCP so they are invisible in this figure. SFCC or SHCP oxygen atoms form an overlayer, which is 2.59 Å (half c) above the Zr surface. (b) Side view of the (3×3) supercell with three Zr layers and Octa12 oxygen atoms. Octahedral sites are located at the center of an octahedron formed by its six nearest Zr neighbors.

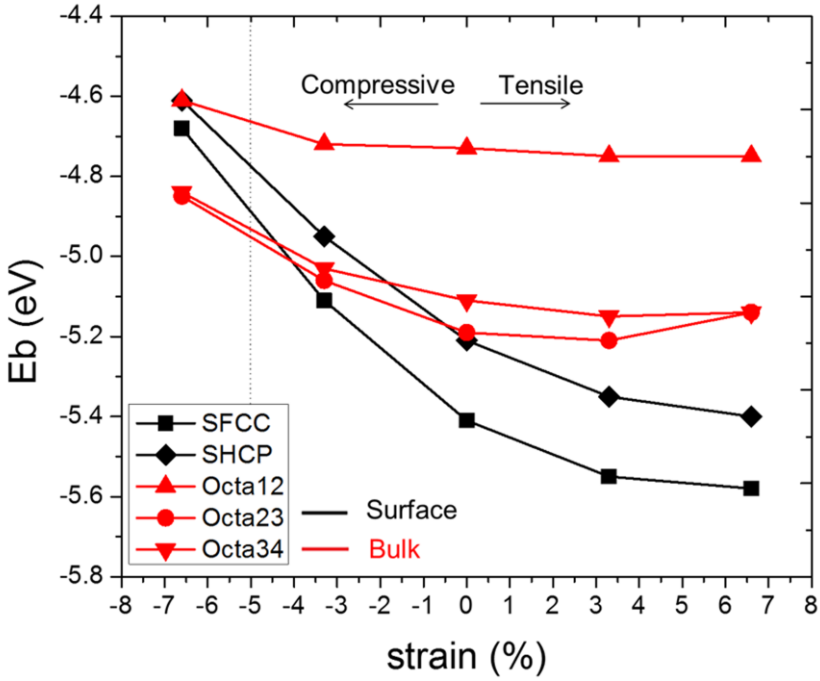

Fig. 2. Oxygen binding energy of different binding sites as a function of strain under θ =1 ML surface coverage. The dotted vertical line at -5.0% strain indicates a possible phase transition from hcp to ω phase of Zr.

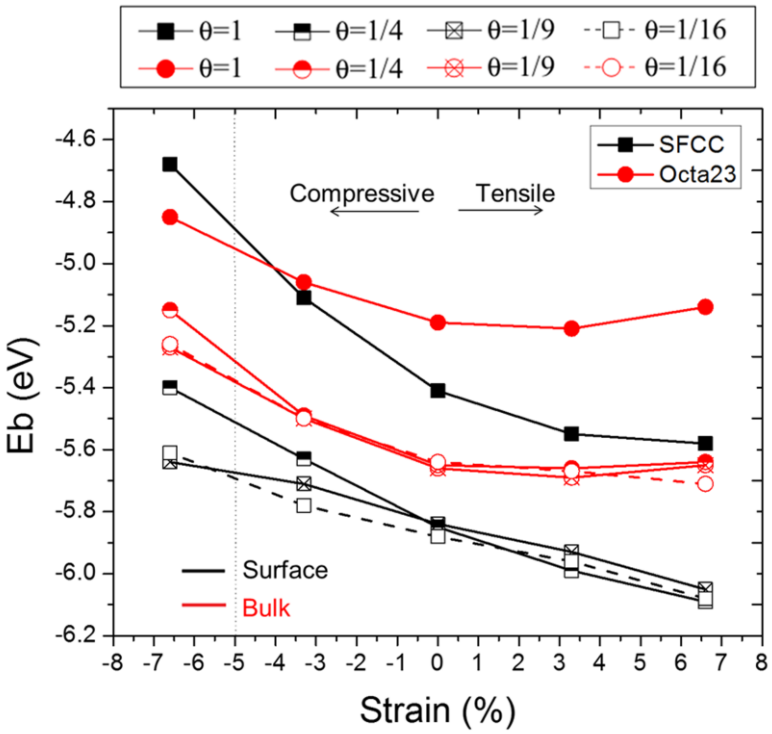

Fig. 3. Oxygen binding energy of SFCC (square) and Octa23 (circle) sites with different oxygen coverage θ. The dotted vertical line at -5.0% strain corresponds to a possible phase transition from hcp to ω phase of Zr.

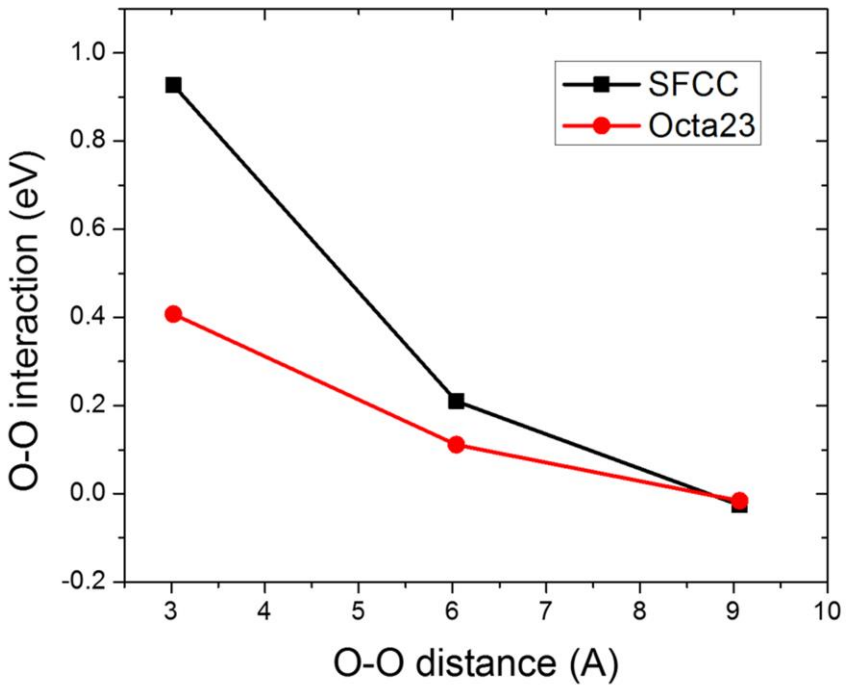

Fig. 4. Interaction energy (eV) of oxygen adsorbates as a function of oxygen distance for SFCC (square) sites and Octa23 (circle) sites. The O-O distance of 9.06 Å, 6.04 Å and 3.02 Å corresponds to oxygen coverage of 1/9 ML, 1/4 ML and 1 ML respectively at strain -6.6%.

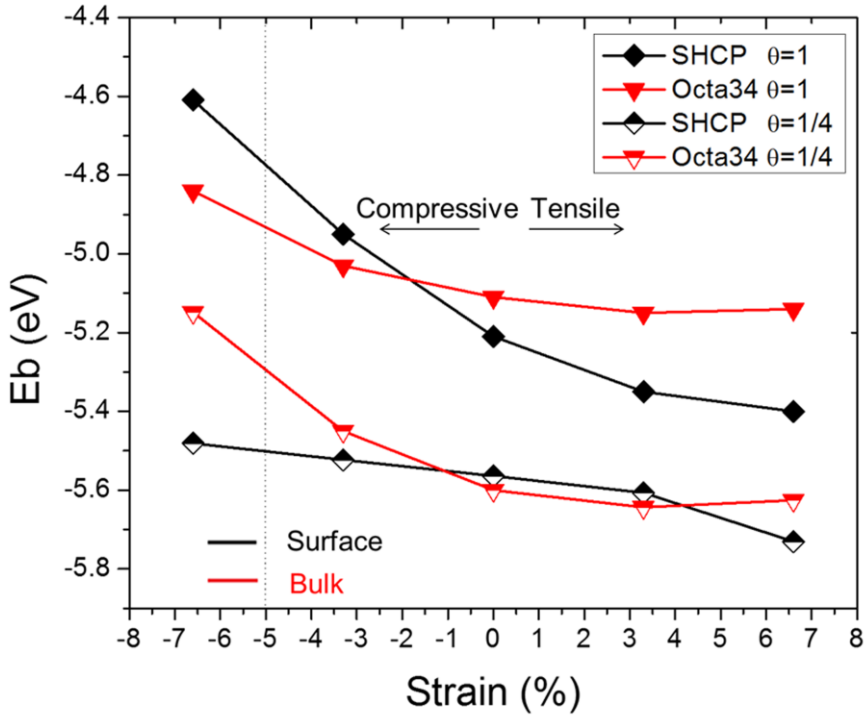

Fig. 5. Oxygen binding energy of SHCP (diamond) and Octa23 (inverted triangle) sites with different oxygen coverage θ. The dotted vertical line at -5.0% strain corresponds to a possible phase transition from hcp to ω phase of Zr.

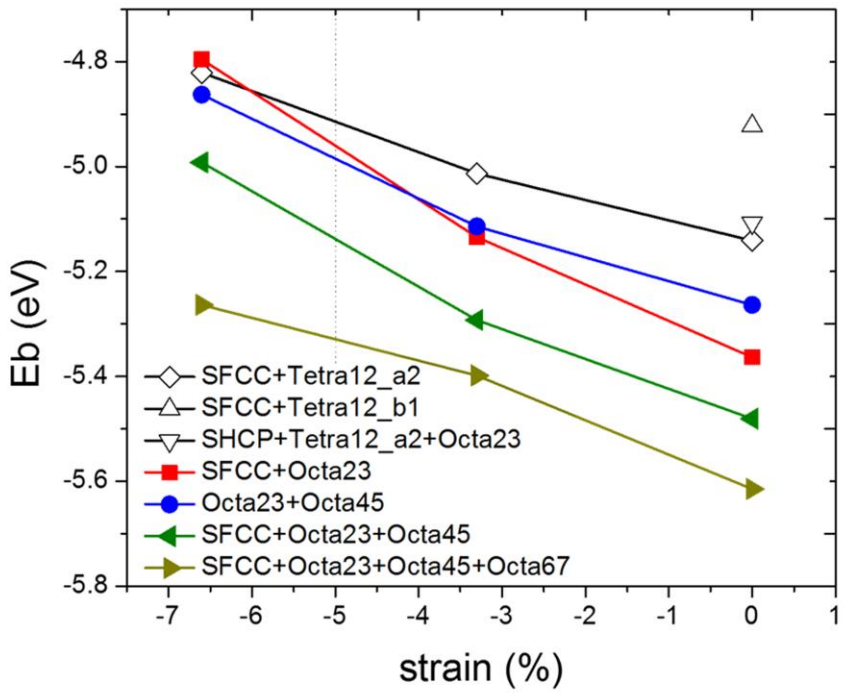

Fig. 6. Oxygen binding energy E_b of selected MLAM configurations under compressive and zero strain conditions when oxygen coverage is θ=2.0 ML. The dotted vertical line at -5.0% strain corresponds to a possible phase transition from hcp to ω phase of Zr. Tetra12_a2 represents tetragonal sites between the first and the second metal layers just above the 2nd Zr layer. Similarly Tetra12_b1 represents tetragonal sites between the first and the second metal layers just below the 1st Zr layer.